

STRATEGIC MODULATION OF THERMAL TO ELECTRICAL ENERGY RATIO PRODUCED FROM PV/T MODULE

ANGES A. AMINOU MOUSSAVOU*, ATANDA K. RAJI, MARCO ADONIS

Center for Distributed Power and Electronics Systems, Cape Peninsula University of Technology (Bellville Campus), Department of Electrical Engineering, Symphony Way, PO Box 1906, Bellville 7535, South Africa

* corresponding author: akdech80@yahoo.fr

ABSTRACT. Several strategies have been developed to enhance the performance of a solar photovoltaic-thermal (PV/T) system in buildings. However, these systems are limited by the cost, complex structure and power consumed by the pump. This paper proposes an optimisation method conversion strategy that modulates the ratio of thermal to electrical energy from the photovoltaic (PV) cell, to increase the PV/T system's performance. The design and modelling of a PV cell was developed in MATLAB/Simulink to validate the heat transfer occurring in the PV cell model, which converts the radiation (solar) into heat and electricity. A linear regression equation curve was used to define the ratio of thermal to electrical energy technique, and the behavioural patterns of various types of power (thermal and electrical) as a function of extrinsic cell resistance (R_{se}). The simulation results show an effective balance of the thermal and electrical power when adjusting the R_{se} . The strategy to modulate the ratio of thermal to electrical energy from the PV cell may optimise the PV/T system's performance. A change of R_{se} might be an effective method of controlling the amount of thermal and electrical energy from the PV cell to support the PV/T system temporally, based on the energy need. The optimisation technique of the PV/T system using the PV cell is particularly useful for households since they require electricity, heating, and cooling. Applying this technique demonstrates the ability of the PV/T system to balance the energy (thermal and electrical) produced based on the weather conditions and the user's energy demands.

KEYWORDS: Cell efficiency, photovoltaic systems, solar photovoltaic-thermal (PV/T) system, modelling and simulation, power production.

1. INTRODUCTION

Renewable energy (RE) originates from the natural processes, which are constantly replenished [1]. RE has been widely promoted in many countries to mitigate the use of electricity from the main grid [2, 3]. RE prevails over fossil fuels because of the high price of oil. Furthermore, it is less harmful to the environment as compared to the traditional power plant [4, 5]. From all the different forms of renewable energy, solar radiation can be used to generate electricity and heat. It offers a sustainable energy supply to domestic and industrial sectors and has demonstrated a promising energy economic development [6, 7]. The combination of photovoltaic and thermal (PV/T) systems is used to generate electricity and thermal energy. The inclusion of the PV/T system in buildings can achieve substantial energy-savings.

Studies on the efficiency of domestic hot water (DHW) distribution systems in buildings have shown that the innovative circulation pipes improve the DHW by reducing the losses by 40% [8]. However, it has been acknowledged that the action of cooling and reheating water in pipes may lead to a thermal fatigue of fixtures and reduce their life cycle [9, 10].

An improvement of the PV/T system composed of PV laminate and absorber with two water channels in which water flows through the upper channel and

returns through the lower channel was reported [11, 12]. This system presents a high thermal efficiency; however, the geometric complexity makes it difficult to manufacture. A conceptual nanofluid-based PV/T system was developed to improve the thermal and electrical efficiency of the system. It was noted that at a temperature of about 62 °C, the controlled flow rate of the nanofluid yielded a total efficiency of 70%, while the electrical and the thermal efficiency were 11% and 59%, respectively [13]. However, this method is costly, suffers from the high-pressure drop and is difficult to hold nanoparticles suspended in the base liquid [14, 15].

An environmentally friendly PV/T system was proposed using a glazed solar collector composed of a PV panel bonded to a metal absorber [16]. The experimental results obtained from the proposed PV/T system show that the PV panel temperature was 45 °C, even in summer, the water temperature circulating within the PV/T was 60 °C based on the flow rate control [16]. A feasibility study of using the PV/T optimisation as a heat source and sink for a reversible heat pump to cool and heat the standard building in three distinct climate zones was evaluated. This PV/T system proved to be technically feasible, and its yearly costs are relatively similar to the traditional

solar cooling systems that use a reversible air-to-water heat pump as the heat and cold source [17].

In view of these findings, it is obvious that an improvement of the PV/T system's performance is needed. This paper proposes an optimisation technique of the PV/T system's performance using the heat flow from the PV cell. Therefore, a controllable self-heating (useful heat) PV cell model using an external parameter is developed to support the PV/T system. The PV cell is partially turned into a useful heat source. Modelling and analysing the PV cell as well as thermal power, electrical power and energy efficiency, were evaluated.

2. THEORETICAL ANALYSIS OF PHOTOVOLTAIC MODULES

Solar photovoltaic technology is highly appreciated due to its abundance and environmental friendliness as compared to other sources. The PV module performance characteristics mainly depend on the ambient temperature and solar radiation. Also, it depends on parameters such as local wind speed, the material and structure of the photovoltaic module, such as glazing-cover transmittance and absorbance [18, 19]. These parameters have an impact on the low energy efficiency conversion.

2.1. INFLUENCE OF SOLAR RADIATION

The overall photovoltaic module performances are typically defined by the standard test conditions (STC), such as radiation, which is 1000 W/m^2 , ambient temperature, 25°C , air mass is 1.5. There is no air velocity near the PV module. However, these performances are completely different once operating in real-world conditions; this difference is due to the perpetual change of the conditions. The PV module performance is associated with the absorption of the solar radiation, the position of the sun through each day and the apparent sun movement during the year [20]. Solar radiation does not reach the Earth's surface intact, because it passes through the Earth's atmosphere. The luminous intensity and its spectrum depend not only on the composition of the atmospheric particles and gases but also on clouds [21–23]. The impact of irradiance on the PV module is given in Equation 1.

$$I_{sc}(T) = I_{sc,ref} [1 + \alpha(T - 25)] \frac{G}{1000 \text{ W/m}^2} \quad (1)$$

Where $I_{sc,ref}$, G , α and T represent the reference short-circuit current at 25°C , global solar radiation on the photovoltaic module surface (W/m^2), a constant temperature coefficient of the module, and the temperature of the photovoltaic module Kelvin (K), respectively.

Photovoltaic modules are made to convert solar radiation into electrical energy. Figure 1 illustrates the influence of the irradiation intensity variation on the PV modules. Figure 1 shows that when the solar

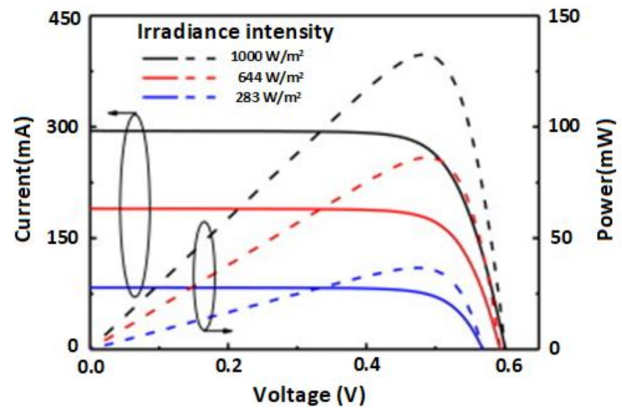


FIGURE 1. The PV cell's characteristics under various solar radiation [24].

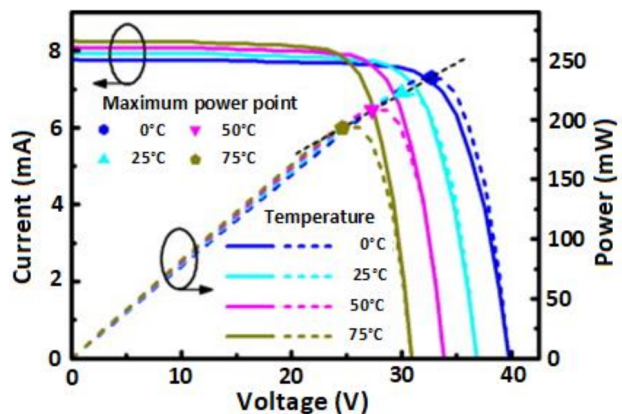


FIGURE 2. The PV module characteristics under various temperatures and an irradiance intensity of 1000 W/m^2 [25].

radiation increases from 233 to 1000 W/m^2 , the maximum power increases from 30 to 120 mW, respectively. The open-circuit voltage of the PV module increases by 0.05 V, while the current stays constant [21, 24].

2.2. INFLUENCE OF THE OPERATING TEMPERATURE OF THE PV MODULE

The temperature rise of the photovoltaic (PV) module reduces its open-circuit voltage (V_{oc}) and decreases the maximum power (P_{mp}). At high temperatures, the formation of electron-holes and the bandgap of the photovoltaic module decreases, while the dark current saturation increases [27–29]. Figure 2 illustrates the $I - V$ characteristics curve of the Photovoltaic performance. The V_{oc} dependence on T is given by the equation below.

$$V_{oc}(T) = V_{oc,ref} [1 + \beta(T_c - T_{ref})] \quad (2)$$

Where $V_{oc,ref}$, β , T_{ref} and T_c represent the reference of the open-circuit voltage, temperature coefficient, the operating temperature of the module and the reference temperature at 25°C , respectively. The derivative of V_{oc} with respect to the temperature and energy

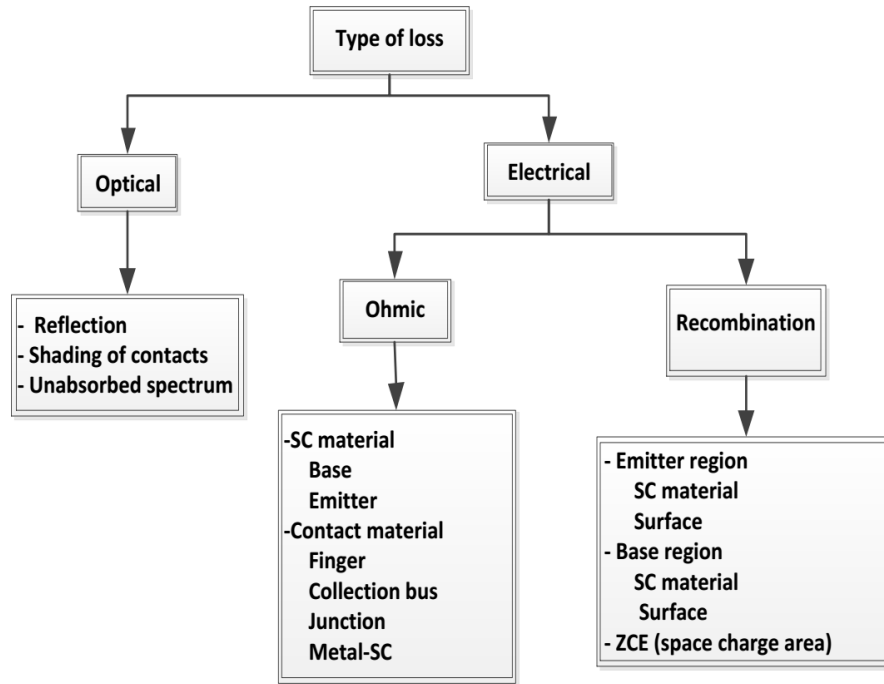


FIGURE 3. Different sources of losses [26].

gap of the semiconductor is expressed in Equation 3:

$$\begin{aligned}
 V_{oc}(T) \frac{dV_{oc}}{dT} &= \frac{V_{oc}}{T} - \frac{\gamma k}{q} - \frac{E_{g0}}{qT} = \\
 &= \frac{1}{T} \left(V_{oc} - \frac{E_{g0}}{q} \right) - \frac{\gamma k}{q} \quad (3)
 \end{aligned}$$

Where γ , k , E_{g0} and q represent the specifics of the temperature coefficient, Boltzmann constant, band gap of the material and electron charge (C), respectively.

The photovoltaic module defined parameters are maximum voltage, open-circuit voltage, maximum current, short-circuit current, maximum power, fill factor and efficiency. In Figure 2, it is denoted that when the temperature increases from 0 to 75 °C, as an immediate consequence, the open-circuit voltage of the photovoltaic module decreases from 40 to 31 V, the maximum power point declines by 55 W and the short-circuit current increases slightly by 0.3 A [30–32]. It is also observed that temperature variations have a marginal effect on the I_{sc} , while having a substantial impact on V_{oc} [28, 33]. The characteristics curve is influenced to different values when photovoltaic modules are exposed to cell damage, radiation change, temperature inequality, local shading and dust, which considerably decreases the output power [30–32].

2.3. LOSSES DUE TO EXTRINSIC AND INTRINSIC IN A SOLAR CELL

Different power losses occur in the PV cell and can be categorised as extrinsic and intrinsic losses, and optical and electrical losses [26, 34] as shown in Figure 3.

Extrinsic loss: This type of losses is caused by reflection, cell damage, shading, series resistance, radiation

change, incomplete collection of generated photocarriers, absorption in the window layer and non-radiative recombination. If the PV module operates under partial shading, the shadow cell is reversely polarised and amplified in the opposite direction; this produces high temperatures because it is charged [35–37].

Intrinsic losses: This type of losses is caused by two factors and the lack of ability of the single-junction solar cell to react adequately to all wavelength spectrums. The solar cell becomes translucent to the photon energy (E_{ph}), and this energy is less than the band gap energy (E_g) of the semiconductor ($E_{ph} < E_g$). However, on condition that the photon energy is higher than the band gap energy of the semiconductor ($E_{ph} > E_g$), the extra energy is dissipated in the form of heat. The loss is also due to the radiative recombination in the solar cell. The common semiconductor material used for the solar cell is silicon, monocrystalline, polycrystalline and amorphous with an efficiency of 20 %, 12 % and 7 %, respectively [38]. The solar cell heating is reversely proportional to the efficiency [29].

3. METHOD AND SIMULATION SET UP

The simulation predicts the thermal behaviour patterns, the total power dissipated (P_d), the power generated and the effectiveness of the PV cell model. This PV model comprises a diode (made of the semiconductor property material of the photovoltaic cell), internal series and internal parallel resistance. It should be noted that for a simulation of a physical phenomenon, like the issue of heat transfer, in Simulink/Simscape, there is a need to establish the calculations of the heat

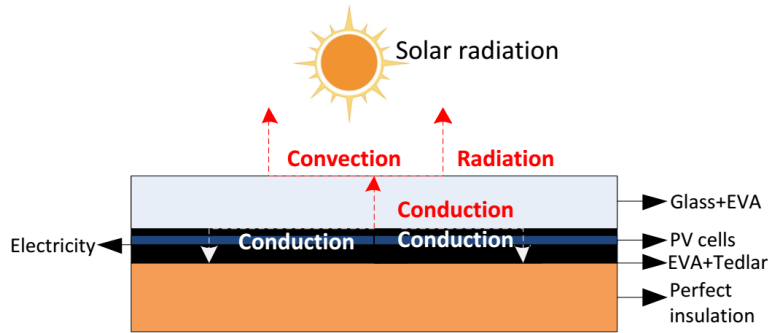


FIGURE 4. Heat transfer characteristics of the PV system.

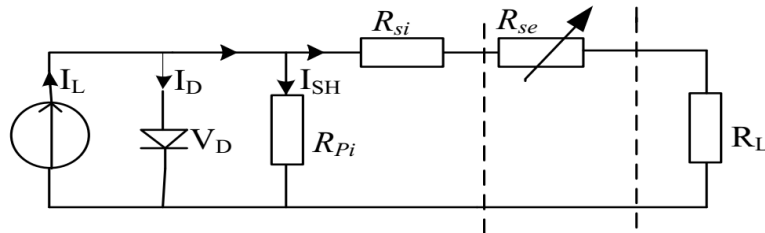


FIGURE 5. Evaluation of PV performance under extrinsic cell resistance.

transfer occurring in this study. Figure 4 depicts the heat transfer characterisation of the PV system.

The following section evaluates the distribution of power dissipated in the PV cells, triggered by extrinsic cell resistance (R_{se}). For this, the electro-thermo-radiative behaviour pattern of the PV cell, for various values of R_{se} ranging from 0 to 100 Ω , were simulated while maintaining other parameters, such as solar radiation at 1000 W/m², ambient temperature at 20 °C and convective heat transfer at 20 W/(m²·K).

The extrinsic cell resistance (R_{se}) is illustrated in Figure 5. The value of R_{se} can be obtained analogically with a variable resistance. It can also be obtained electronically by applying a voltage on the FET’s gate pin resistance. The channel resistance of the FET is a function of the gate-source voltage. By increasing the reverse biasing, the resistance increases.

In this study, the PV modules parameters are listed in Table 1 and Table 2. The entire PV system consists of two PV arrays assumed to perform identically and in a parallel configuration; the system has a capacity of 3.24 kW_p at 1000 W/m².

4. SIMULATION RESULTS AND DISCUSSION

The PV cell model is analysed and discussed to better appreciate the optimisation technique of the PV/T system using the PV cell. The simulation is performed under stable conditions.

4.1. PV CELL POWER DISSIPATION AS A FUNCTION OF R_{se}

The parameters representing the PV cell’s internal properties are comprised of a diode, series resistance and parallel resistance. The model is assessed based

on extrinsic cell resistance. Figure 6 shows an increment in the total Pd curve, from 990 to 3490 W, as R_{se} increases. Series resistance marginally increases, while parallel resistance remains virtually the same. A considerable amount of the total power dissipation is attributed to the diode (because of the recombination current of the semiconductor material property used to make the PV cell model), ranging from 750 to 3480 W. The series and parallel resistance resistivity losses decrease as less current flow through them.

A substantial reverse current occurred in the PV cells in the form of heat. This reverse current leads to a Pd and then to a local overheating and turns into heat by conduction. The PV thermal resistance varies based on the width of the material and its thermal resistivity. Figure 6 shows an increase in the total Pd of the PV cell, from 990 to 3490 W, as R_{se} increases. This increase in R_{se} will reduce the fill factor and then decrease the maximum-power point of PV cells. The graph in Figure 6 is consistent with those obtained from previous studies [39–41]. However, here, the R_{se} causes the restricted conductivity of the terminal material used. The following trend can be elucidated: the R_{se} constrains a partial conversion of the PV output into a useful thermal energy. This study focuses on the internal heat generation and electrical power generation of the PV cell based on the R_{se} . The technique relies on the linear regression equation curve to model the behaviour of different types of power as a function of R_{se} in the PV cell being studied.

Component	Parameter	Value
PV modules	Cell type	Mono-crystalline
	Packing factor	0.91
	Conversion efficiency	16 %
	Module peak power	3.25 kW
	Maximum voltage, V_m	255 V
	Maximum current, I_m	12.4 A
	Open circuit voltage, V_{oc}	310 V
	Short circuit current, I_{sc}	14.64 A
	Series resistance R_{si} / cell	0.0042 Ω
Parallel resistance R_{pi} /cell	10.1 Ω	

TABLE 1. PV module parameters.

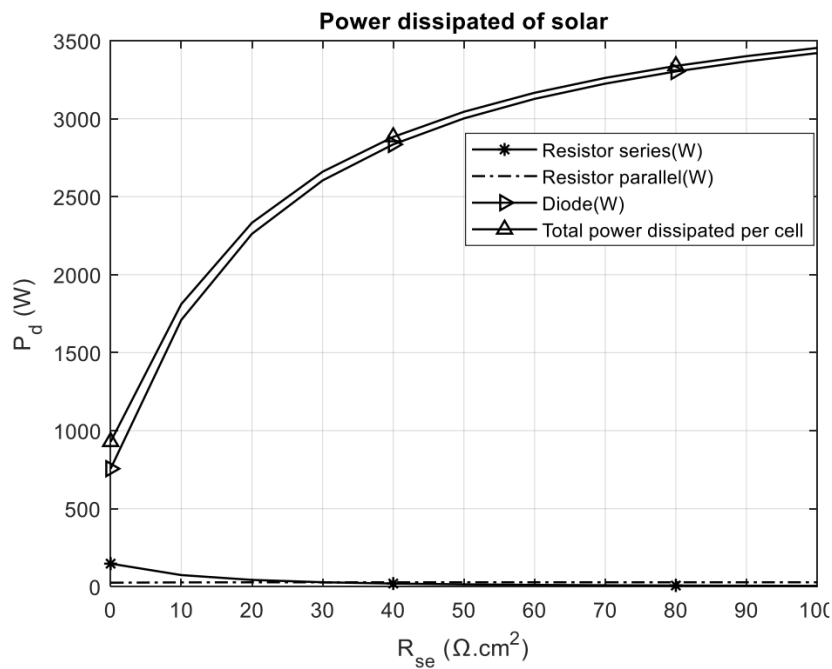


FIGURE 6. Dissipated power by PV cell versus R_{se} .

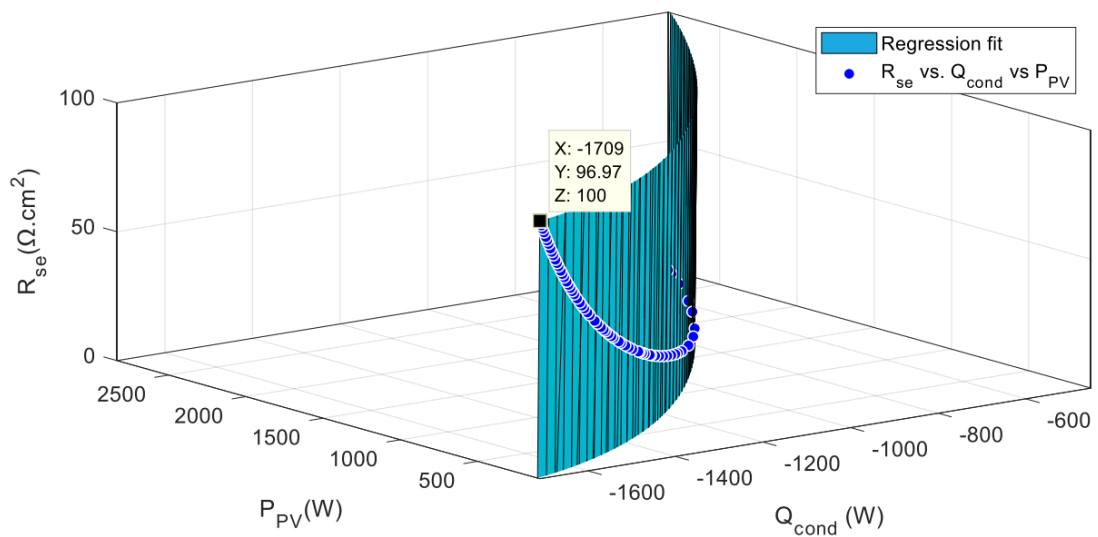


FIGURE 7. R_{se} according to the power generated and heat by conduction of the PV module.

	PV module type
Absorbance α	0.8
Emissivity ϵ	0.75
Thermal conductivity	840
Thickness δ	0.003
Temperature coefficient	0.000905
Energy gap EG	1.11

TABLE 2. Optical parameters of PV cells.

4.2. ESTIMATION OF HEAT TRANSFER BY CONDUCTION AND GENERATED PV POWER AS A FUNCTION OF R_{se}

The synthesis of the results, illustrated in Figure 7 in 3D, shows a standardised map of R_{se} as a function of the heat transfer by conduction, and the generated PV power. The normalised yields are plotted on this map, which includes the polynomial surface of the model. By adjusting R_{se} , the equivalent values of the electrical power generated and electrical power dissipated by heat conduction is determined. Figure 7 presents the heat generated by conduction (Q_{cond}) within the PV cell. Q_{cond} rises from 425 to 1715 W (in magnitude) as R_{se} moves from 0 to 100 Ω . This heat is ascribed to electrical power dissipated in the PV cell, and part of the dissipated power turns into useful energy within the PV cell. However, the temperature difference is the main impetus behind the conductive heat flow in a material with a given thermal resistance, and the transfer is governed by the Fourier law.

It can be seen in Figure 7 that the generated PV power decreases as R_{se} increases. The power rapidly (exponentially) falls from 2800 W to 260 W when R_{se} increases from 0 to 50 Ω , and beyond 50 Ω , the power decreases slower from 255 W to 110 W. The power degradation of a PV cell is due to recombination according to R_{se} variation, leading to electrical power dissipation in the form of heat by conduction. These outcomes are in concurrence with those acquired by other authors, where the rise of R_{se} is attributed to dust particles on the PV model [42–44]. Contrary to other studies, R_{se} is used to proportionally influence the electrical power and power dissipation of the PV cell.

A polynomial model appropriately represents the graphical model of the results. It can be used to predict and interpret the PV cell's performance. The confidence intervals and the means of the linear regression equation for the graphical model result was derived. The estimation graph is expressed by Equation 4.

$$R_{se}(Q_{cond}P_{PV}) = p00 + p10 \cdot Q_{cond} + p01 \cdot P_{PV} + p20 \cdot Q_{cond}^2 + p11 \cdot Q_{cond} \cdot P_{PV} + p02 \cdot P_{PV}^2 \quad (4)$$

where $p00$, $p10$, $p01$, $p20$, $p11$ and $p02$ are coefficients, Q_{cond} is the thermal transfer coefficient by conduc-

tion (W), P_{PV} is the generated PV power and R_{se} is the external series resistance (Ω).

Table 3 describes the polynomial interpretation of the surface plot result of the heat conduction and PV power as a function of R_{se} in Figure 7; The estimation curve is expressed by Equation 4. To find the optimal power (electrical or thermal), computation of the coefficient of determination (R^2) is 0.9998 and RMSE is 0.4791 for any selected value of R_{se} .

4.3. CONVECTION AND RADIATION HEAT GENERATED BY THE PV CELL

Figure 8 illustrates a steady increase in convection (Q_{conv}) from 3100 W to 5300 W when the R_{se} value increases from 0 to 100 Ω , as the heat is carried to the atmosphere. The impact of heat on the PV cell is caused by the high electrical power dissipation, and the heat loss by the conduction happening in the PV cell. The thermal loss by Q_{conv} increases faster when R_{se} is in the range between 0 and 50 Ω ; nonetheless, Q_{conv} is slowed down and approaches saturation when R_{se} is higher than 50 Ω .

Figure 9 presents the incremental change of radiation (Q_{rad}) from 350 W to 660 W when R_{se} increases from 0 to 100 Ω . The PV cell emits radiation based on its temperature. Also, the losses depend on the absorptivity of the covering glass.

The outcomes shown in Figure8 and Figure 9 demonstrate that the growth of the heat loss by Q_{conv} is higher than that in Q_{rad} . Both were assessed as positive values, which shows that they are taken away into the ambient environment. At the same time, the Q_{cond} is measured as a negative value in Figure 7. This negative value indicates that the Q_{cond} is directed mostly inside the PV cell. Comparing the heat transfer happening in the PV cell, Q_{conv} , Q_{cond} and Q_{rad} , varied by 2200 W, 1290 W and 310 W, respectively, as R_{se} differed by 100 Ω . Some others discussed the convection, conduction and radiation heat transfer occurring in the PV module, here, the effect of R_{se} is included in this paper [45–48].

4.4. THE PV CELL TEMPERATURE UNDER R_{se} VARIATION

Figure10 illustrates the logarithmic growth of Tc as a function of R_{se} . As R_{se} varies from 0 to 50 Ω , the temperature Tc rises from 45 to 59 $^{\circ}\text{C}$, and as R_{se} value increases from 50 to 100 Ω , Tc increases slowly from 59 to 62 $^{\circ}\text{C}$. The rise in Tc leads to a build-up of electrical Pd in the form of heat in Figure6. Most of the previous works show that the R_{se} expands by the rise of the PV cell temperature [41]. Inversely, here, the PV cell temperature is controlled by R_{se} , to improve the PV/T system's thermal efficiency.

4.5. PV CELL ELECTRICAL EFFICIENCY UNDER R_{se} VARIATION

Figure 11 presents the PV cell electrical efficiency dependence on R_{se} . The PV cell electrical efficiency

Description of Equation 4	Goodness of fit
$R_{se}(Q_{cond}P_{PV}) = p00 + p10 \cdot Q_{cond} + p01 \cdot P_{PV} + p20 \cdot Q_{cond}^2 + p11 \cdot Q_{cond} \cdot P_{PV} + p02 \cdot P_{PV}^2$ where x is normalised by mean -1385 and std 328.5 and where y is normalised by mean 561.3 and std 662.5. Coefficients (with 95 % confidence bounds): $p00 = -829(-982.3, -675.8)$ $p10 = 3100(2542, 3658)$ $p01 = -4467(-5261, -3673)$ $p20 = 965.3(808.8, 1122)$ $p11 = -223.2(-242.9, -203.5)$ $p02 = 145.4(127.7, 163.1)$	SSE: 12.85 R-square: 0.9998 Adjusted R-square: 0.9997 RMSE: 0.4791

TABLE 3. Linear model Poly22 of Figure 7.

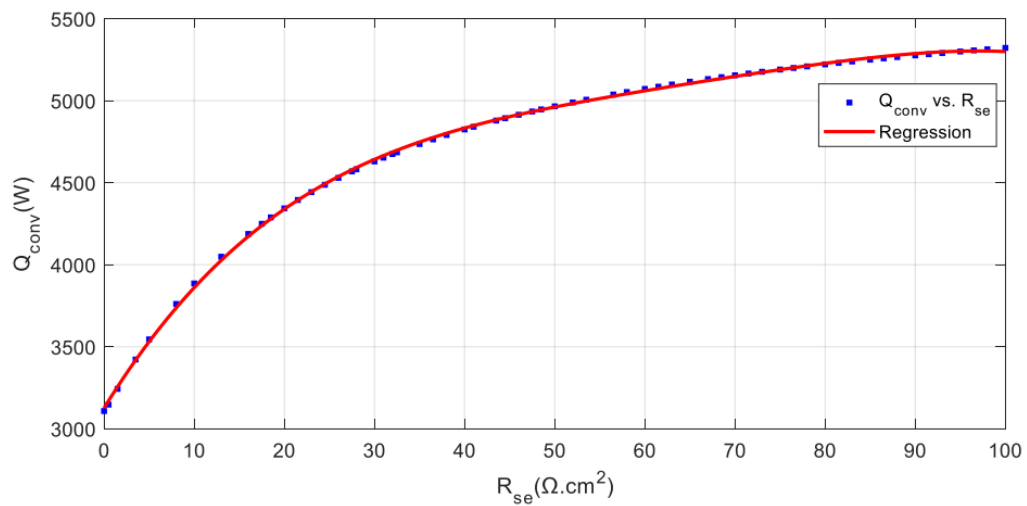


FIGURE 8. Convection heat transfer versus R_{se} .

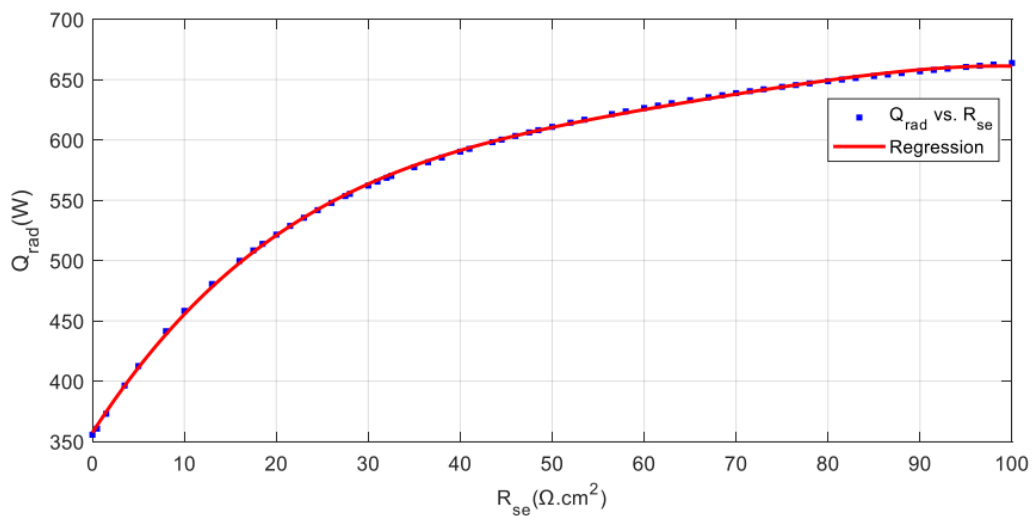


FIGURE 9. Radiation heat transfer versus R_{se} .

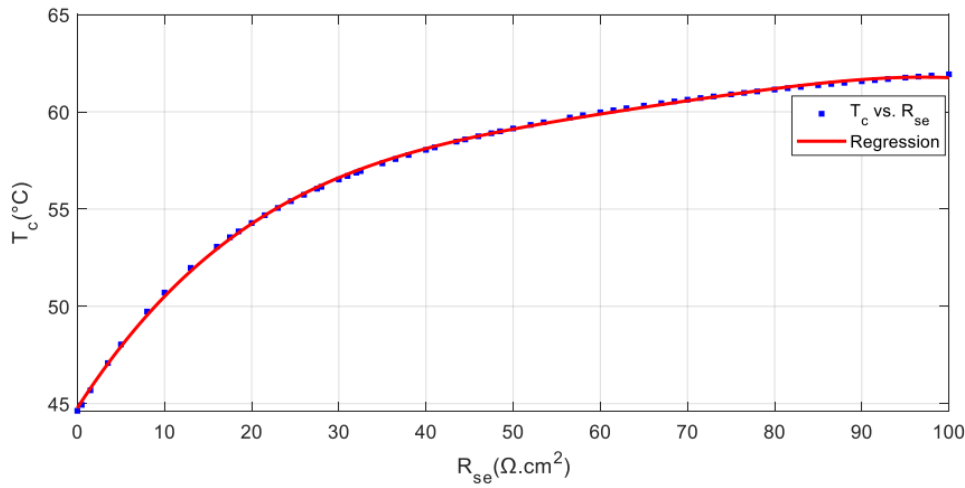


FIGURE 10. PV cell temperature versus R_{se} .

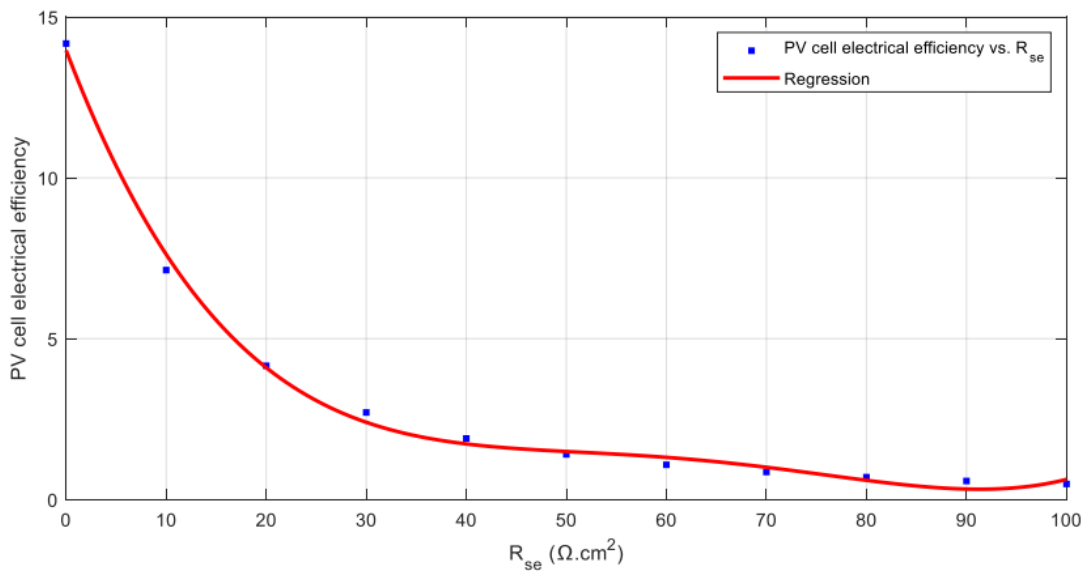


FIGURE 11. PV cell electrical efficiency dependence on R_{se} .

quickly (exponentially) falls from 14.2 % to 2.5 % when R_s increases from 0 to 50 Ω , and above 50 Ω , the efficiency slowly decreases from 2.5 % to 1.5 %. This was observed to be in agreement with the results reported by similar studies [41, 49]. The degradation of the PV cell power was due to the power dissipation in the form of heat shown in Figure 6.

4.6. GENERATED POWER THROUGH TIME

Here, the heat by conduction corresponds to the useful thermal energy. In the electrical power and the heat by conduction in the PV module vary based on R_{se} , mainly due to the power dissipation.

Here, the heat by conduction corresponds to the useful thermal energy. As shown in Figure 7, the electrical power and the heat by conduction in the PV module vary, based on R_{se} , mainly due to the power dissipation.

This indicates that, if the R_{se} is selected, PV will only deliver electrical power and thermal power under

a given condition. For example, it is observed in Figure 12 that when R_{se} is 0 Ω , the electrical and thermal power at the steady-state is 2835 W and 450 W, respectively. The electrical power is prioritised. While in Figure 13, when R_{se} is to set 20 Ω , the electrical and thermal power at the steady-state is 831 W and 1150 W, respectively. The electrical power is degraded to prioritise the useful thermal energy. However, the R_{se} is used to control the energy of the PV module. These findings are consistent with similar previous studies [42, 43].

5. CONCLUSION

The design and modelling of a PV cell system were carried out in MATLAB/Simulink to validate the heat transfer occurring in the PV cell model. The PV cell's output is partially converted into useful thermal energy (the internal heat generation) for domestic hot water supply and space heating. A change of R_{se} might be an effective method of controlling the amount

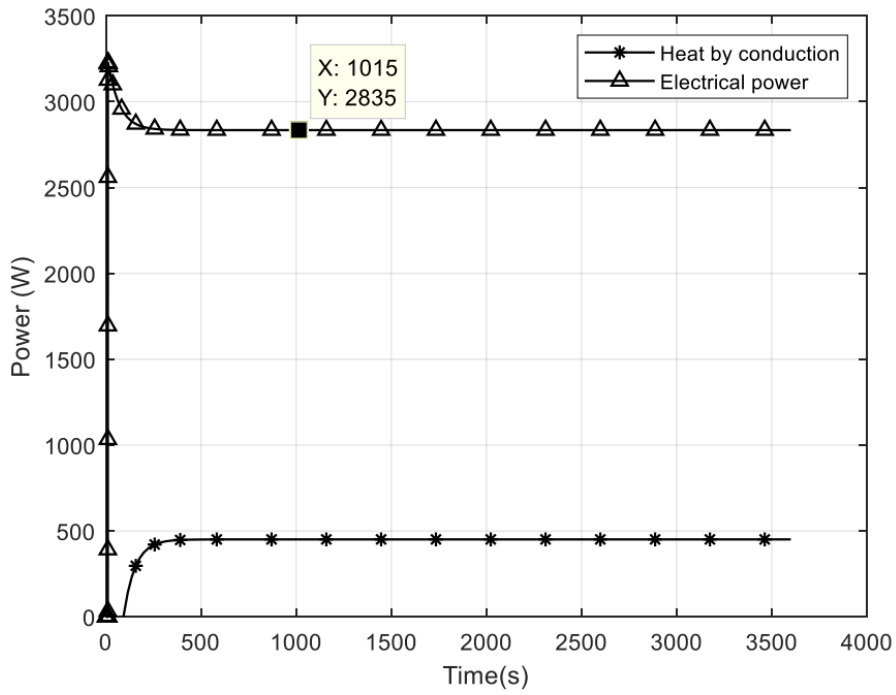


FIGURE 12. Generated powers from PV cell when R_{se} is 0Ω .

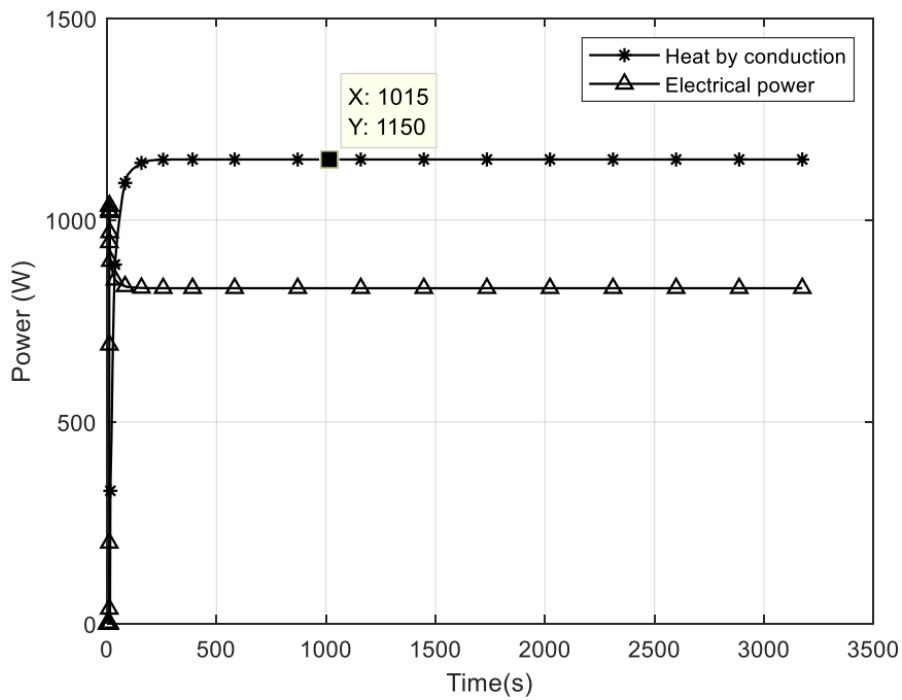


FIGURE 13. Generated powers from PV cell when R_{se} is 20Ω .

of thermal and electrical energy from the PV cell. The technique is determined by a linear regression equation curve to model the behavioural patterns of various types of power (thermal and electrical) as a function of R_{se} .

These findings are particularly useful for household water-heating systems. R_{se} may be adjusted to produce supplementary heat while the fluid carries the produced heat to the load.

A further research will develop a model that incorporates the absorber pipe affixed at the rear of the PV cell model, all together linked to a hydraulic pump and storage device. The optimisation technique that modulates the ratio of thermal to the electrical energy generated from the PV cell may be used to optimise the combined PV/T system's performance.

REFERENCES

- [1] N. El Bassam, P. Maegaard, M. L. Schlichting. Chapter six - Energy basics, resources, global contribution and applications. In *Distributed Renewable Energies for Off-Grid Communities*, pp. 85 – 90. Elsevier, 2013. <https://doi.org/10.1016/B978-0-12-397178-4.00006-2>.
- [2] W.-C. Lu. Greenhouse gas emissions, energy consumption and economic growth: a panel cointegration analysis for 16 Asian countries. *International journal of environmental research and public health* **14**(11):1436, 2017. <https://doi.org/10.3390/ijerph14111436>.
- [3] A. A. A. Moussavou, M. Adonis, A. K. Raji. Microgrid energy management system control strategy. In *2015 International Conference on the Industrial and Commercial Use of Energy (ICUE)*, pp. 147 – 154. 2015. <https://doi.org/10.1109/ICUE.2015.7280261>.
- [4] A. N. Nunes. Energy changes in Portugal. An overview of the last century. *Méditerranée Revue géographique des pays méditerranéens/Journal of Mediterranean geography* (130), 2018. <https://doi.org/10.4000/mediterranee.10113>.
- [5] A. Stocker, A. Großmann, R. Madlener, M. I. Wolter. Sustainable energy development in Austria until 2020: Insights from applying the integrated model “e3. at”. *Energy policy* **39**(10):6082 – 6099, 2011. <https://doi.org/10.1016/j.enpol.2011.07.009>.
- [6] D. Banks, J. Schäffler. *The potential contribution of renewable energy in South Africa*. Sustainable Energy & Climate Change Project, 2006.
- [7] A. Chel, G. Kaushik. Renewable energy technologies for sustainable development of energy efficient building. *Alexandria Engineering Journal* **57**(2):655 – 669, 2018. <https://doi.org/10.1016/j.aej.2017.02.027>.
- [8] B. Bøhm. Production and distribution of domestic hot water in selected Danish apartment buildings and institutions. Analysis of consumption, energy efficiency and the significance for energy design requirements of buildings. *Energy Conversion and Management* **67**:152 – 159, 2013. <https://doi.org/10.1016/j.enconman.2012.11.002>.
- [9] G. Y. Chuang, Y. M. Ferng. Experimentally investigating the thermal mixing and thermal stripping characteristics in a T-junction. *Applied Thermal Engineering* **113**:1585 – 1595, 2017. <https://doi.org/10.1016/j.applthermaleng.2016.10.157>.
- [10] R. Tunstall, D. Laurence, R. Prosser, A. Skillen. Large eddy simulation of a T-Junction with upstream elbow: The role of Dean vortices in thermal fatigue. *Applied Thermal Engineering* **107**:672 – 680, 2016. <https://doi.org/10.1016/j.applthermaleng.2016.07.011>.
- [11] J.-H. Kim, J.-T. Kim. The experimental performance of an unglazed PVT collector with two different absorber types. *International Journal of Photoenergy* **2012**, 2012. <https://doi.org/10.1155/2012/312168>.
- [12] H. A. Zondag. Flat-plate PV-Thermal collectors and systems: A review. *Renewable and Sustainable Energy Reviews* **12**(4):891 – 959, 2008. <https://doi.org/10.1016/j.rser.2005.12.012>.
- [13] Z. Xu, C. Kleinstreuer. Concentration photovoltaic-thermal energy co-generation system using nanofluids for cooling and heating. *Energy Conversion and Management* **87**:504 – 512, 2014. <https://doi.org/10.1016/j.enconman.2014.07.047>.
- [14] A. H. A. Al-Waeli, M. T. Chaichan, H. A. Kazem, et al. Numerical study on the effect of operating nanofluids of photovoltaic thermal system (PV/T) on the convective heat transfer. *Case studies in thermal engineering* **12**:405 – 413, 2018. <https://doi.org/10.1016/j.csite.2018.05.011>.
- [15] P. K. Nagarajan, J. Subramani, S. Suyambazhahan, R. Sathyamurthy. Nanofluids for solar collector applications: A review. *Energy Procedia* **61**:2416 – 2434, 2014. <https://doi.org/10.1016/j.egypro.2014.12.017>.
- [16] K. Terashima, H. Sato, T. Ikaga. Development of an environmentally friendly PV/T solar panel. *Solar Energy* **199**:510 – 520, 2020. <https://doi.org/10.1016/j.solener.2020.02.051>.
- [17] R. Braun, M. Haag, J. Stave, et al. System design and feasibility of trigeneration systems with hybrid photovoltaic-thermal (PVT) collectors for zero energy office buildings in different climates. *Solar Energy* **196**:39 – 48, 2020. <https://doi.org/10.1016/j.solener.2019.12.005>.
- [18] O. Dupre, B. Niesen, S. De Wolf, C. Ballif. Field performance versus standard test condition efficiency of tandem solar cells and the singular case of perovskites/silicon devices. *The journal of physical chemistry letters* **9**(2):446 – 458, 2018. <https://doi.org/10.1021/acs.jpcclett.7b02277>.
- [19] L. Hernández-Callejo, S. Gallardo-Saavedra, V. Alonso-Gómez. A review of photovoltaic systems: Design, operation and maintenance. *Solar Energy* **188**:426 – 440, 2019. <https://doi.org/10.1016/j.solener.2019.06.017>.
- [20] V. Perraki, P. Kounavis. Effect of temperature and radiation on the parameters of photovoltaic modules. *Journal of Renewable and Sustainable Energy* **8**(1):013102, 2016. <https://doi.org/10.1063/1.4939561>.
- [21] M. R. Maghami, H. Hizam, C. Gomes, et al. Power loss due to soiling on solar panel: A review. *Renewable and Sustainable Energy Reviews* **59**:1307 – 1316, 2016. <https://doi.org/10.1016/j.rser.2016.01.044>.

- [22] J. Page. Chapter IIA-1 - The Role of Solar-Radiation Climatology in the Design of Photovoltaic Systems. In *Practical Handbook of Photovoltaics*, pp. 573 – 643. Academic Press, Boston, second edition edn., 2012. <https://doi.org/10.1016/B978-0-12-385934-1.00017-9>.
- [23] T. Markvart, L. Castañer (eds.). *Practical Handbook of Photovoltaics: Fundamentals and Applications*. Elsevier, 2013. <https://doi.org/10.1016/B978-1-85617-390-2.X5000-4>.
- [24] C. Xiao, X. Yu, D. Yang, D. Que. Impact of solar irradiance intensity and temperature on the performance of compensated crystalline silicon solar cells. *Solar Energy Materials and Solar Cells* **128**:427 – 434, 2014. <https://doi.org/10.1016/j.solmat.2014.06.018>.
- [25] J.-C. Wang, Y.-L. Su, J.-C. Shieh, J.-A. Jiang. High-accuracy maximum power point estimation for photovoltaic arrays. *Solar Energy Materials and Solar Cells* **95**(3):843 – 851, 2011. <https://doi.org/10.1016/j.solmat.2010.10.032>.
- [26] A. R. Jha. *Solar Cell Technology and Applications*. Auerbach Publications, 2009. <https://doi.org/10.1201/9781420081787>.
- [27] F. Fertig, S. Rein, M. Schubert, W. Warta. Impact of junction breakdown in multi-crystalline silicon solar cells on hot spot formation and module performance. In *26th European Photovoltaic Solar Energy Conference and Exhibition*, pp. 1168 – 1178. 2011. <https://doi.org/10.4229/26thEUPVSEC2011-2DO.3.1>.
- [28] P. Singh, N. M. Ravindra. Temperature dependence of solar cell performance - an analysis. *Solar energy materials and solar cells* **101**:36 – 45, 2012. <https://doi.org/10.1016/j.solmat.2012.02.019>.
- [29] J. Zaraket, T. Khalil, M. Aillerie, et al. The Effect of Electrical stress under temperature in the characteristics of PV Solar Modules. *Energy Procedia* **119**:579 – 601, 2017. <https://doi.org/10.1016/j.egypro.2017.07.083>.
- [30] J. C. Teo, R. H. G. Tan, V. H. Mok, et al. Impact of partial shading on the pv characteristics and the maximum power of a photovoltaic string. *Energies* **11**(7):1860, 2018. <https://doi.org/10.3390/en11071860>.
- [31] A. J. Swart, P. E. Hertzog. Varying percentages of full uniform shading of a PV module in a controlled environment yields linear power reduction. *Journal of Energy in Southern Africa* **27**(3):28 – 38, 2016.
- [32] P. Arjyadhara, S. M. Ali, J. Chitralkha. Analysis of solar PV cell performance with changing irradiance and temperature. *International Journal of Engineering and Computer Science* **2**(1):214 – 220, 2013.
- [33] P. Löper, D. Pysch, A. Richter, et al. Analysis of the temperature dependence of the open-circuit voltage. *Energy Procedia* **27**:135 – 142, 2012.
- [34] C. H. Henry. Limiting efficiencies of ideal single and multiple energy gap terrestrial solar cells. *Journal of Applied Physics* **51**(8):4494 – 4500, 1980. <https://doi.org/10.1063/1.328272>.
- [35] G. Trzmiel, D. Głuchy, D. Kurz. The impact of shading on the exploitation of photovoltaic installations. *Renewable Energy* **153**:480 – 498, 2020. <https://doi.org/10.1016/j.renene.2020.02.010>.
- [36] A. M. Humada, F. B. Samsuri, M. Hojabria, et al. Modeling of photovoltaic solar array under different levels of partial shadow conditions. In *16th International Power Electronics and Motion Control Conference and Exposition*, pp. 461 – 465. 2014. <https://doi.org/10.1109/EPEPEMC.2014.6980535>.
- [37] F. Lu, S. Guo, T. M. Walsh, A. G. Aberle. Improved pv module performance under partial shading conditions. *Energy Procedia* **33**:248 – 255, 2013. <https://doi.org/10.1016/j.egypro.2013.05.065>.
- [38] L. A. Kosyachenko. *Solar Cells - Thin-Film Technologies*, chap. Thin-Film Photovoltaics as a Mainstream of Solar Power Engineering, pp. 1 – 40. IntechOpen Limited, London, 2011. <https://doi.org/10.5772/39070>.
- [39] D. Kiermasch, L. Gil-Escrig, H. J. Bolink, K. Tvingstedt. Effects of masking on open-circuit voltage and fill factor in solar cells. *Joule* **3**(1):16 – 26, 2019. <https://doi.org/10.1016/j.joule.2018.10.016>.
- [40] H. A. Koffi, A. A. Yankson, A. F. Hughes, et al. Determination of the series resistance of a solar cell through its maximum power point. *African Journal of Science, Technology, Innovation and Development* **12**(6):699 – 702, 2020. <https://doi.org/10.1080/20421338.2020.1731073>.
- [41] M. Wolf, H. Rauschenbach. Series resistance effects on solar cell measurements. *Advanced Energy Conversion* **3**(2):455 – 479, 1963. [https://doi.org/10.1016/0365-1789\(63\)90063-8](https://doi.org/10.1016/0365-1789(63)90063-8).
- [42] P. G. Kale, K. K. Singh, C. Seth. Modeling effect of dust particles on performance parameters of the solar PV module. In *2019 Fifth International Conference on Electrical Energy Systems*, pp. 1 – 5. 2019. <https://doi.org/10.1109/ICEES.2019.8719298>.
- [43] A. Hussain, A. Batra, R. Pachauri. An experimental study on effect of dust on power loss in solar photovoltaic module. *Renewables: Wind, Water, and Solar* **4**(1):9, 2017. <https://doi.org/10.1186/s40807-017-0043-y>.
- [44] K. Dastoori, G. Al-Shabaan, M. Kolhe, et al. Charge measurement of dust particles on photovoltaic module. In *8th International Symposium on Advanced Topics in Electrical Engineering*, pp. 1 – 4. 2013. <https://doi.org/10.1109/ATEE.2013.6563411>.
- [45] R. Vaillon, O. Dupré, R. B. Cal, M. Calaf. Pathways for mitigating thermal losses in solar photovoltaics. *Scientific reports* **8**:13163, 2018.
- [46] M. Hammami, S. Torretti, F. Grimaccia, G. Grandi. Thermal and performance analysis of a photovoltaic module with an integrated energy storage system. *Applied Sciences* **7**(11):1107, 2017. <https://doi.org/10.3390/app7111107>.
- [47] R. Masoudi Nejad. A survey on performance of photovoltaic systems in iran. *Iranian (Iranica) Journal of Energy & Environment* **6**(2):77 – 85, 2015. <https://doi.org/10.5829/idosi.ijee.2015.06.02.01>.
- [48] J. A. Duffie, W. A. Beckman. *Solar Engineering of Thermal Processes*. Wiley, New York, 1991.
- [49] P. Singh, N. Ravindra. Analysis of series and shunt resistance in silicon solar cells using single and double exponential models. *Emerging Materials Research* **1**:33 – 38, 2012. <https://doi.org/10.1680/emr.11.00008>.